scientific reports

Check for updates

OPEN

Optical coupling control of isolated mechanical resonators

F. E. Onah[1,2], B. R. Jaramillo-Ávila[3]✉, F. H. Maldonado-Villamizar[4] & B. M. Rodríguez-Lara[5]

We present a Hamiltonian model describing two pairs of mechanical and optical modes under standard optomechanical interaction. The vibrational modes are mechanically isolated from each other and the optical modes couple evanescently. We recover the ranges for variables of interest, such as mechanical and optical resonant frequencies and naked coupling strengths, using a finite element model for a standard experimental realization. We show that the quantum model, under this parameter range and external optical driving, may be approximated into parametric interaction models for all involved modes. As an example, we study the effect of detuning in the optical resonant frequencies modes and optical driving resolved to mechanical sidebands and show an optical beam splitter with interaction strength dressed by the mechanical excitation number, a mechanical bidirectional coupler, and a two-mode mechanical squeezer where the optical state mediates the interaction strength between the mechanical modes.

Optomechanical systems provide a versatile platform for quantum optics experiments and applications, including optical bi-stability[1,2], damping and anti-damping of mechanical motion in microwave-coupled mechanical resonators[3,4], optically-assisted cooling of mechanical oscillations[5–9], and optomechanically induced transparency[10,11], for example. Additionally, optomechanical devices in various configurations provide an excellent platform to study optically mediated interactions between mechanical resonators[12–14]. This lead to several phenomenon such as P and PT symmetry in mechanical resonators[15–17], and dark mode control[9]. Optomechanical systems are a promising platform[18–23] to build sensors[19,24] and quantum information transducers[25,26] relying on the effect of electromagnetic radiation pressure on the vibrational modes of mechanical objects[27,28]; for example, suspended micromirrors, membranes, microtoroids, microsphere resonators, micromembranes in superconducting circuits, 2D photonic crystals, photonic crystal nanobeams, and cold atoms in optical cavities[4]. Additionally, some of these platforms allow for further coupling between two or more optomechanical cavities, increasing the number of plausible applications for these systems[29].

Recent advances in optomechanical cooling provide access to both mechanical and optical ground states and open the door to a wider range of low excitation number experiments[30]. Optomechanical systems in the quantum regime may find use in quantum technologies. For example, in quantum sensing and metrology, controlling the interaction of mechanical oscillators may lead to the engineering of two-mode squeezed states[31–37], or the development of mechanical couplers[38,39] needed for mechanical interferometers. In quantum information platforms, they may serve as transducers from microwave to optical spectrum[40,41] or mechanical memories[42,43].

We are interested in the quantum dynamical description of two mechanically isolated vibrational modes, each one interacting with its own optical mode under standard optomechanical coupling. We introduce evanescent coupling between optical modes that allows for optical control of mechanical coupling under optical sideband driving. We present a finite element modeling analysis of plausible physical realizations for our model in order to recover parameter ranges that may inform our analysis of the dynamics. Next, we introduce the quantum mechanical model and show that it is possible to define a reference frame where it takes the form of a parametric Hamiltonian where all mechanical and optical modes interact. In this reference frame, it becomes straightforward to realize that it is possible to induce and control the interaction of the mechanical modes by external optical sideband driving. Then, we explore on-resonance driving of identically fabricated optical cavities and show that the effective model is that of an optical beam splitter where the coupling strength is modified by the state of the vibrational modes. We show that red sideband driving of the optical cavities with detuning equal

[1]Tecnológico de Monterrey, Escuela de Ingeniería y Ciencias, Ave. Eugenio Garza Sada 2501, Monterrey, N.L. 64849, Mexico. [2]The Division of Theoretical Physics, Physics and Astronomy, University of Nigeria Nsukka, Nsukka Campus, Nsukka, Enugu State, Nigeria. [3]CONAHCYT-CICESE, Unidad Monterrey, Alianza Centro 504, PIIT, Apodaca, Nuevo Leon 66629, Mexico. [4]CONAHCYT-Instituto Nacional de Astrofísica, Óptica y Electrónica, Calle Luis Enrique Erro No. 1, Sta. Ma. Tonantzintla, Pue. C.P. 72840, Mexico. [5]Universidad Politécnica de Pachuca, Carr. Pachuca-Cd. Sahagún Km.20, Ex-Hda. Santa Bárbara, Zempoala 43830, Hidalgo, Mexico. ✉email: bjaramillo@cicese.mx

to the mechanical frequency produces different effects depending on the detuning between the optical cavities. If the resonant frequency detuning between the optical cavities is equal to the difference between the mechanical resonant frequencies, optically mediated mechanical mode coupling appears. If it is equal to the sum of the mechanical resonant frequencies, optical mediated parametric mechanical coupling appears. In both cases, the optical state affects the coupling strength between the mechanical vibrational modes, we numerically explore these dynamics.

Finite element model

We are interested in a standard experimental optomechanical setup; a silica nanobeam with an engraved one-dimensional photonic defect cavity[44–46]. For the sake of simplicity, we consider a periodic array composed by 75 rectangular cells where a quadratic reduction in size for the middle 15 cells introduces a defect[44]. We take each regular cell with length 360 nm (x-axis), width 1400 nm (y-axis), and thickness 220 nm (z-axis) and use finite element modeling (FEM) to find the principal optical and mechanical modes at $(2\pi)\,204\times10^{12}$ rad/s and $(2\pi)\,2.23\times10^{9}$ rad/s, in that order, in good agreement with experimental results[44]. Radiation pressure may induce a mechanical deformation that modifies the geometry of each optical cavity and, in consequence, its characteristic frequency, leading to optomechanical coupling. Photonic crystal nanobeams of these scales lead to bare optomechanical couplings of the order of $g\sim(2\pi)\,10^{6}$ rad/s[46]. These devices need to be pumped with an external laser whose power may vary from a few to hundreds of thousands of nanowatts, see supplementary material in Ref.[46], leading to laser-to-cavity coupling rates of the order of tens of 10^{6} rad/s[46] and to pump rates between $\Omega_{\rm min}\sim(2\pi)\,10^{9}$ rad/s and $\Omega_{\rm max}\sim(2\pi)\,10^{11}$ rad/s.

In order to explore theoretically the optical coupling between two of these structures, we place two identical nanobeams parallel to each other and vary their separation. We use two possible configurations, one nanobeam on top of the other, Fig. 1a and two nanobeams side-by-side, Fig. 1b. In both configurations, we consider the mechanical modes of each nanobeam isolated. The optical modes localized in each photonic defect cavity have evanescent fields outside its structure. These fields may overlap with the cavity in the neighboring nanobeam, producing optical coupling. The optical coupling has a roughly decaying exponential behavior as a function of the separation between the nanobeams. We quantify the coupling strength between the two fundamental optical modes by looking at their odd and even combinations in the two nanobeam structures. Let us define the frequency of the odd (even) mode as λ_+ (λ_-). Its value is above (below) the frequency of a single beam fundamental mode λ_0 and we approximate it as $\lambda_+=\lambda_0+\gamma$ ($\lambda_-=\lambda_0-\gamma$), where the parameter γ is the optical coupling strength. Our finite element model provides us with numerical values for the even and odd frequencies at various nanobeam separation values s and, in consequence, allows us to extract an optical coupling strength $\gamma(s)$ as a function of the separation, Fig. 2. As expected, we find an exponential decay of the optical coupling strength as the separation between the beams s increases. For the on-top configuration, we find simple exponential decay, Fig. 2a , for the optical coupling as a function of s and, in contrast, the side-by-side configuration follows fourth-order exponential decay in s, Fig. 2b. Additionally, the on-top configuration provides stronger optical coupling than the side-by-side configuration but might be experimentally difficult to fabricate. The latter provides a much weaker optical coupling but its fabrication is more feasible[47].

Quantum mechanical model

The quantum mechanical description for our optomechanical system, composed by two isolated mechanical resonators, each supporting an optical mode with evanescent coupling between them,

$$\frac{\hat{H}}{\hbar}=\sum_{j=1}^{2}\left[\omega_j\hat{a}_j^{\dagger}\hat{a}_j+\nu_j\hat{b}_j^{\dagger}\hat{b}_j-g_j\hat{a}_j^{\dagger}\hat{a}_j\left(\hat{b}_j^{\dagger}+\hat{b}_j\right)+\Omega_j\cos\left(\omega_{dj}t\right)\left(\hat{a}_j^{\dagger}+\hat{a}_j\right)\right]+\gamma\left(\hat{a}_1^{\dagger}\hat{a}_2+\hat{a}_1\hat{a}_2^{\dagger}\right),\qquad(1)$$

is given in terms of the creation (annihilation) operators for the optical $\hat{a}_j^{\dagger}$ ($\hat{a}_j$) and mechanical $\hat{b}_j^{\dagger}$ ($\hat{b}_j$) modes, the optical and mechanical mode frequencies are ω_j and ν_j, in that order, the optomechanical coupling, optical driving, and optical coupling strengths are g_j, Ω_j, and γ, respectively, the driving fields frequencies are ω_{d_j} with

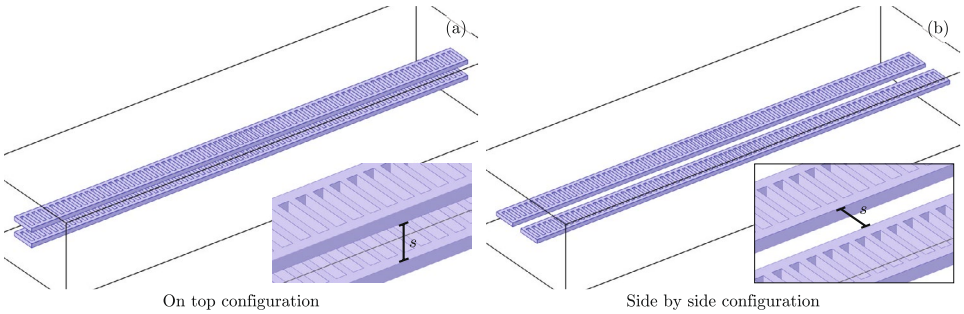

Figure 1. (**a**) On-top and (**b**) side-by-side configurations coupling optical modes in two isolated optomechanical photonic crystal nanobeams.

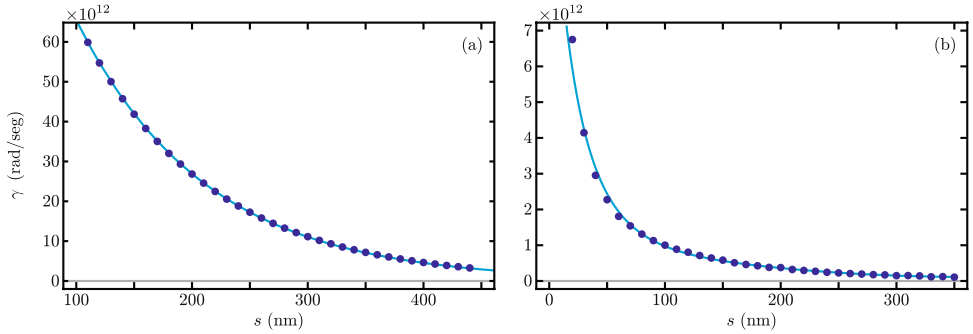

Figure 2. Coupling between the fundamental optical modes in two identical optomechanical photonic crystal nanobeams as a function of the gap between the nanobeams s for the (**a**) on-top and (**b**) side-by-side configurations. Dots show results from FEM and solid curves fit a simple exponential decay for the on-top configuration and fourth-order polynomial exponential decay for the side-by-side configuration.

$j = 1, 2$. Moving into the reference frame defined by free optical fields, $|\psi_0\rangle = e^{-i\sum_j \omega_j \hat{a}_j^\dagger \hat{a}_j t}|\psi_1\rangle$, allows us to apply a rotating wave approximation to disregard terms moving at fast optical frequencies, $\omega_j + \omega_{dj}$, and consider an effective Hamiltonian,

$$\frac{\hat{H}_1}{\hbar} \approx \sum_{j=1}^{2}\left[\nu_j \hat{b}_j^\dagger \hat{b}_j - g_j \hat{a}_j^\dagger \hat{a}_j\left(\hat{b}_j^\dagger + \hat{b}_j\right) + \frac{1}{2}\Omega_j\left(\hat{a}_j^\dagger e^{i\Delta_j t} + \hat{a}_j e^{-i\Delta_j t}\right)\right] + \gamma\left[\hat{a}_1^\dagger \hat{a}_2 e^{i\delta t} + \hat{a}_1 \hat{a}_2^\dagger e^{-i\delta t}\right], \tag{2}$$

where the optical driving term depends on the detuning between the resonant and driving frequencies, $\Delta_j = \omega_j - \omega_{dj}$, and the coupling terms by the detuning between resonant frequencies, $\delta = \omega_1 - \omega_2$. Now, a displacement of the mechanical modes proportional to the excitation number in the optical modes followed by moving to the frame defined by the free mechanical term, $|\psi_1\rangle = e^{-\sum_j \alpha_j \hat{a}_j^\dagger \hat{a}_j\left(\hat{b}_j^\dagger - \hat{b}_j\right)} e^{-i\sum_j \nu_j \hat{b}_j^\dagger \hat{b}_j t}|\psi_2\rangle$ with $\alpha_j = -g_j/\nu_j$, yields an effective Hamiltonian,

$$\frac{\hat{H}_2}{\hbar} = \hat{H}_K + \hat{H}_{om} + \hat{H}_{oc} \tag{3}$$

with three components, an effective Kerr term,

$$\hat{H}_K = -\sum_j \frac{g_j^2}{\nu_j}\left(\hat{a}_j^\dagger \hat{a}_j\right)^2, \tag{4}$$

for the optical modes dependent on the ratio between the optomechanical coupling squared to the mechanical resonant frequency. The optomechanical detuning term converts into parametric coupling between each mechanical resonator mode and its corresponding inscribed optical cavity mode,

$$\hat{H}_{OM} = \frac{1}{2}\sum_{j=1}^{2}\Omega_j e^{-\frac{1}{2}\alpha_j^2}\sum_{p,q=0}^{\infty}\frac{(-1)^q \alpha_j^{p+q}}{p!q!}\left[\hat{a}_j^\dagger \hat{b}_j^{\dagger p}\hat{b}_j^q e^{i[\Delta_j + (p-q)\nu_j]t} + \hat{a}_j \hat{b}_j^{\dagger q}\hat{b}_j^p e^{-i[\Delta_j + (p-q)\nu_j]t}\right], \tag{5}$$

feasible of control by the detuning between the external driving and the optical cavity. The optical coupling term converts into parametric coupling between optical and mechanical modes,

$$\begin{aligned}\hat{H}_{OC} = \gamma e^{-\frac{1}{2}(\alpha_1^2+\alpha_2^2)}\sum_{r,s,u,v=0}^{\infty}\frac{(-1)^{s+u}\alpha_1^{r+s}\alpha_2^{u+v}}{r!s!u!v!}\Big[&\hat{a}_1^\dagger \hat{a}_2 \hat{b}_1^{\dagger r}\hat{b}_1^s \hat{b}_2^{\dagger u}\hat{b}_2^v e^{i[\delta + (r-s)\nu_1 + (u-v)\nu_2]t} \\ &+ \hat{a}_1 \hat{a}_2^\dagger \hat{b}_1^{\dagger s}\hat{b}_1^r \hat{b}_2^{\dagger v}\hat{b}_2^u e^{-i[\delta + (r-s)\nu_1 + (u-v)\nu_2]t}\Big],\end{aligned} \tag{6}$$

feasible of control by the detuning between the optical cavities resonant frequencies, $\delta = \omega_1 - \omega_2$. Thus, we may control the parametric processes between each mechanical resonator and its inscribed optical mode via external driving fields, aiming for $\Delta_j + (p-q)\nu_j = 0$, but the parametric processes between isolated mechanical modes, mediated by the coupled optical modes, is controlled by the detuning between the optical cavities resonant frequencies, aiming for $\delta + (r-s)\nu_1 + (u-v)\nu_2 = 0$, which is provided by the fabrication itself.

Mechanically controlled optical beam splitter

Let us drive the optical cavities on-resonance, $\Delta_j = 0$, such that the optomechanical coupling terms satisfy the optical pumping control condition $\Delta + (p-q)\nu_j = 0$ with $p = q$. In addition, if we consider the optical cavities identical, $\delta = 0$, such that the optical coupling terms with $r = s$ and $u = v$ satisfy the condition $\delta + (r-s)\nu_1 + (u-v)\nu_2 = 0$, we end up with a driven nonlinear optical beam splitter Hamiltonian,

$$\hat{H}_{NBS} = \sum_j \left\{ -\frac{g_j^2}{\nu_j}\left(\hat{a}_j^\dagger \hat{a}_j\right)^2 + \frac{\Omega_j}{2}\hat{F}[j,1,0]\left(\hat{a}_j^\dagger + \hat{a}_j\right)\right\} + \gamma \hat{F}[1,1,0]\hat{F}[2,1,0]\left(\hat{a}_1^\dagger \hat{a}_2 + \hat{a}_1 \hat{a}_2^\dagger\right), \tag{7}$$

where the driving strength and the optical coupling strength depend on the auxiliary Hermitian operator function,

$$\hat{F}[j,p,q] = \left(-\frac{g_j}{\nu_j}\right)^q e^{-\frac{1}{2}\left(\frac{g_j}{\nu_j}\right)^2} {}_1\mathrm{F}_1\left[-\hat{b}_j^\dagger \hat{b}_j; p; \left(\frac{g_j}{\nu_j}\right)^2\right], \tag{8}$$

given in terms of the optomechanical coupling strength g_j, the resonant mechanical frequency ν_j, the mechanical excitation number $\hat{b}_j^\dagger \hat{b}_j$, and the confluent hypergeometric function ${}_1\mathrm{F}_1[a; b; z]$.

For the typical optomechanical coupling strength to resonant frequency ratio in nanobeams, $g_j/\nu_j \ll 1$, the auxiliary Hermitian operator function may be approximated to a form,

$$\hat{F}[j,p,q] \simeq \left(\frac{g_j}{\nu_j}\right)^q \left[1 - \left(\frac{1}{2} + \frac{\hat{b}_j^\dagger \hat{b}_j}{p}\right)\left(\frac{g_j}{\nu_j}\right)^2 + \mathcal{O}\left(\frac{g_j}{\nu_j}\right)^4\right], \tag{9}$$

whose leading order depends on the mechanical excitation number $\hat{b}_j^\dagger \hat{b}_j$; for example,

$$\hat{F}[j,1,0] \approx 1 - \left(\frac{1}{2} + \hat{b}_j^\dagger \hat{b}_j\right)\left(\frac{g_j}{\nu_j}\right)^2, \tag{10}$$

a sufficiently small mechanical excitation number, $\hat{F}[j,1,0] \approx 1$, provides us with an effective driven nonlinear optical beam splitter,

$$\hat{H}_{NBS} \approx \sum_j \left\{ -\frac{g_j^2}{\nu_j}\left(\hat{a}_j^\dagger \hat{a}_j\right)^2 + \frac{\Omega_j}{2}\left(\hat{a}_j^\dagger + \hat{a}_j\right)\right\} + \gamma\left(\hat{a}_1^\dagger \hat{a}_2 + \hat{a}_1 \hat{a}_2^\dagger\right), \tag{11}$$

with constant parameters in the so-called Rabi regime, $g_j^2/\nu_j \ll \gamma$, where the spectrum of the system without driving, $\Omega = 0$, is linear. As a result, we may approximate the system,

$$\hat{H}_{NBS} \approx \sum_j \frac{\Omega_j}{2}\left(\hat{a}_j^\dagger + \hat{a}_j\right) + \gamma\left(\hat{a}_1^\dagger \hat{a}_2 + \hat{a}_1 \hat{a}_2^\dagger\right), \tag{12}$$

and recover a standard optical beam splitter with driving. In the future, it may be possible to have larger optomechanical coupling strength that allows exploring the nonlinear regimes available in the model. Our mechanically isolated configuration may explore these nonlinear regimes in the case where the nanobeams are sufficiently apart from each other, such that the optical coupling is minimal, making it a trivial scenario.

Figure 3 shows the Lindblad evolution of the mean value of the optical mode excitation number, $\langle \hat{a}_j^\dagger \hat{a}_j \rangle$ with $j = 1, 2$ using the full master equation in the simplified reference frame provided by our Hamiltonian in Eq. (7) under the leading order approximation for the auxiliary Hermitian operator function $\hat{F}[j,p,q]$ in Eq. (9). We must emphasize that optical excitation numbers remain unchanged by the reference frame transformations. While mechanical excitation numbers are affected by these reference frame transformations, the numerical difference between the simplified and laboratory reference frames remains numerically small of the order of $\lesssim 10^{-7}$. In this numerical simulation we introduce the following optomechanical parameters, $\nu_1 = \nu_2 = \nu, \Omega_1/\nu = \Omega_2/\nu = 10$, $\Delta_1/\nu = \Delta_2/\nu = 0$, $\gamma/\nu = 400$, $\delta/\nu = 0$, $\gamma_{o,j}/\nu = 0.09$ and $\gamma_{m,j}/\nu = 1.5 \times 10^{-5}$. The optical and mechanical loss rates $\gamma_{o,j}$ and $\gamma_{m,j}$, in that order, are consistent with experimental results[45] for devices similar to our Finite Element Model. The interplay between experimental bare optomechanical couplings and loss rates in current experimental systems make it impossible to observe this phenomenon in the laboratory at the time. In order to do so, the bare optomechanical couplings must increase and the loss rates decrease. Considering current loss rates, the optomechanical couplings need increase five hundred times in order to see the effects described in this section, $g_1/\nu = g_2/\nu = 0.2$. Here, we opted for this approach rather than user smaller loss rates aiming for small evolution times that allow a full master equation treatment using Linblad formalism. For the optical component of the initial state, we use initial states with one excitation entangled between the two optical modes, to produce oscillations between them. For the mechanical component of the initial state, we use two distinct states to compare the effect of mechanical excitation numbers. One initial state has zero mechanical excitation $|\psi(0)\rangle = \left[\cos\left(\frac{\pi}{3}\right)|1,0\rangle_{\mathrm{opt}} + \sin\left(\frac{\pi}{3}\right)|0,1\rangle_{\mathrm{opt}}\right]|0,0\rangle_{\mathrm{mec}}$, Fig. 3a and b. The other initial state has one mechanical excitation $|\psi(0)\rangle = \left[\cos\left(\frac{\pi}{3}\right)|1,0\rangle_{\mathrm{opt}} + \sin\left(\frac{\pi}{3}\right)|0,1\rangle_{\mathrm{opt}}\right]|0,1\rangle_{\mathrm{mec}}$, Fig. 3c and d. For long evolution times, we

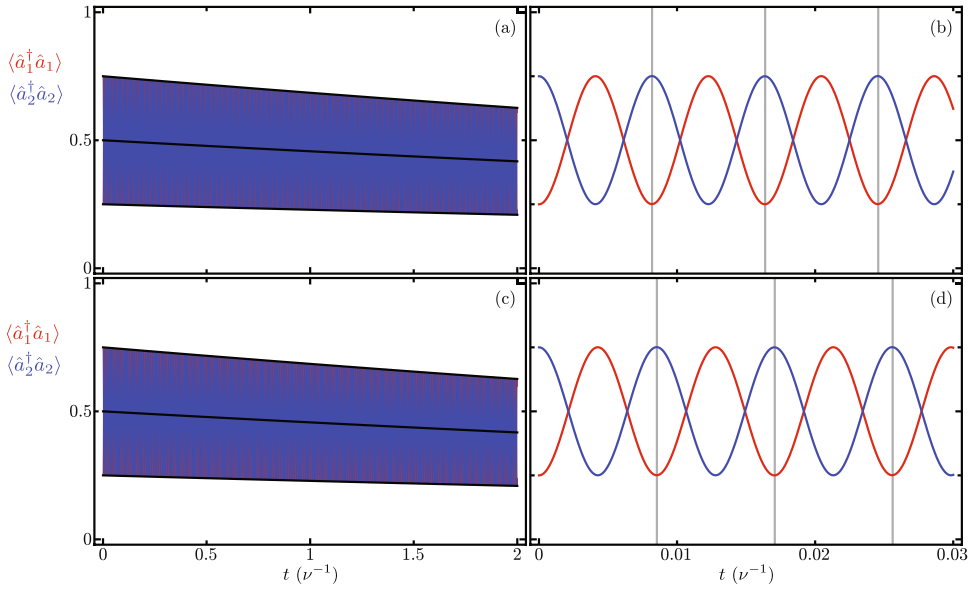

Figure 3. Time evolution of the optical mode excitation number, $\langle \hat{a}_j^\dagger \hat{a}_j \rangle$ with $j = 1, 2$, for initial states (**a**,**b**) $|\psi(0)\rangle = \left[\cos(\frac{\pi}{3})|1,0\rangle_{\text{opt}} + \sin\left(\frac{\pi}{3}\right)|0,1\rangle_{\text{opt}}\right]|0,0\rangle_{\text{mec}}$ and (**c**,**d**) $|\psi(0)\rangle = \left[\cos\left(\frac{\pi}{3}\right)|1,0\rangle_{\text{opt}} + \sin\left(\frac{\pi}{3}\right)|0,1\rangle_{\text{opt}}\right]|0,1\rangle_{\text{mec}}$ for (**a**) and (**c**) long and (**b**) and (**c**) short evolution times. The exchange period between optical modes is indicated by vertical gray lines.

observe decay due to optical losses, Fig. 3a and c. For short evolution times, Fig. 3b and d, we observe optical excitation exchange with temporal period,

$$\tau = 2\pi \left\{ \gamma e^{-\frac{1}{2}\left(\frac{g_1}{\nu_1}\right)^2} e^{-\frac{1}{2}\left(\frac{g_2}{\nu_2}\right)^2} {}_1\mathrm{F}_1\left[-\langle \hat{b}_1^\dagger \hat{b}_1 \rangle; 1; \left(\frac{g_1}{\nu_1}\right)^2\right] {}_1\mathrm{F}_1\left[-\langle \hat{b}_2^\dagger \hat{b}_2 \rangle; 1; \left(\frac{g_2}{\nu_2}\right)^2\right] \right\}^{-1}, \tag{13}$$

that depends on the mechanical excitation number, $\langle \hat{b}_j^\dagger \hat{b}_j \rangle$ with $j = 1, 2$. We find good agreement between our closed-form expression and the temporal periods obtained from numerical experiments, vertical lines in Fig. 3b and d. Figure 4 displays the effective coupling governing the optical excitation exchange in our mechanically controlled optical beam splitter, where $2\pi/\tau$ is the effective coupling corresponding to an excitation exchange with temporal period τ. The effective coupling depends both on the bare optomechanical couplings, $g_j = g_1 = g_2$, and the mechanical occupation numbers, $\langle \hat{b}_j^\dagger \hat{b}_j \rangle$. A larger mechanical occupation number produces a smaller value for the effective coupling. This numerical simulation uses the same numerical parameters as those in Fig. 3, except that the bare optomechanical coupling is variable and the losses are neglected, their effect on the effective coupling is very small.

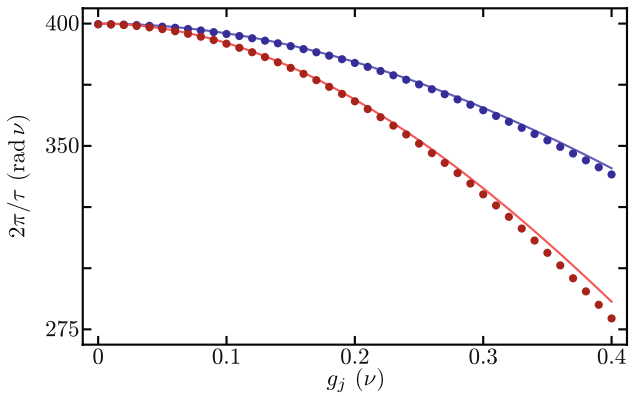

Figure 4. Effective coupling for optical excitation exchange as a function of the bare optomechanical couplings $g_j = g_1 = g_2$. Blue (red) curves correspond to systems with zero (one) total mechanical excitation. Dots correspond to the effective coupling obtained from numerical experiments and solid curves to our closed-form expressions.

Optically controlled mechanical coupler

Let us drive the red sideband of the optical cavities, $\Delta_j = \nu_j$, such that the optomechanical coupling terms with $q = p + 1$ satisfy the optical pumping control condition $\Delta_j + (p - q)\nu_j = 0$. In addition, we consider the optical cavities with a detunning equivalent to $\delta = -\nu_1 + \nu_2$, such that the optical coupling terms with $r = s + 1$ and $v = u + 1$ satisfy the condition $\delta + (r - s)\nu_1 + (u - v)\nu_2 = 0$. Under these considerations, the effective Hamiltonian describing the system,

$$\begin{aligned}\hat{H}_{OMC} = &-\sum_j \left\{ \frac{g_j^2}{\nu_j}\left(\hat{a}_j^\dagger \hat{a}_j\right)^2 + \frac{\Omega_j}{2}\left(\hat{a}_j^\dagger F[j,2,1]\hat{b}_j + \hat{a}_j \hat{b}_j^\dagger F[j,2,1]\right)\right\} \\ &- \gamma\left\{\hat{a}_1^\dagger \hat{a}_2 \hat{b}_1^\dagger \hat{F}[1,2,1]\hat{F}[2,2,1]\hat{b}_2 + \hat{a}_1 \hat{a}_2^\dagger \hat{b}_2^\dagger \hat{F}[1,2,1]\hat{F}[2,2,1]\hat{b}_1\right\}\end{aligned} \tag{14}$$

becomes a nonlinear coupler of mechanical and optical modes where the excitation transfer between optical modes is accompanied by the transfer of mechanical excitation. Here, we used the auxiliary Hermitian operator function $\hat{F}[j,p,q]$ defined before.

A first-order approximation using the coupling and pump rates ranges available in the experimental setups discussed in our finite element model leads to the following effective model,

$$\hat{H}_{OMC} \approx -\sum_j \left[\frac{g_j^2}{\nu_j}\left(\hat{a}_j^\dagger \hat{a}_j\right)^2 + \Omega_{eff_j}\left(\hat{a}_j^\dagger \hat{b}_j + \hat{a}_j \hat{b}_j^\dagger\right)\right] - \Gamma_{\text{eff}}\left(\hat{a}_1^\dagger \hat{a}_2 \hat{b}_1^\dagger \hat{b}_2 + \hat{a}_1 \hat{a}_2^\dagger \hat{b}_2^\dagger \hat{b}_1\right), \tag{15}$$

with the effective linear optomechanical coupling strength $\Omega_{eff_j} = \Omega g_j/(2\nu_j)$ and the parametric coupling strength $\Gamma_{\text{eff}} = \gamma g_1 g_2/(\nu_1 \nu_2)$ mixing all optical and mechanical modes. For the nanobeams under consideration and using the maximum feasible pump rate of 10^5 nW, Ω_{eff_j} becomes the leading coupling, which is of the order of tens of megahertz. The second leading rate is Γ_{eff}, which is of the order of a few megahertz or fractions of a megahertz. Finally, the coupling g_j^2/ν_j is the smallest of the three, of the order of a few kilohertz. Such that we may approximate,

$$\hat{H}_{OMC} \approx -\sum_j \Omega_{eff_j}\left(\hat{a}_j^\dagger \hat{b}_j + \hat{a}_j \hat{b}_j^\dagger\right) - \Gamma_{\text{eff}}\left(\hat{a}_1^\dagger \hat{a}_2 \hat{b}_1^\dagger \hat{b}_2 + \hat{a}_1 \hat{a}_2^\dagger \hat{b}_2^\dagger \hat{b}_1\right), \tag{16}$$

the dynamics with a linear parametric model that associates the exchange of optical excitation with that of mechanical excitation.

Figure 5 (Fig. 6) show the Schrödinger equation time evolution with a non Hermitian Hamiltonian of the optomechanical excitation numbers in both nanobeams under the effective nonlinear coupled Hamiltonian in Eq. (14). Where, again, we use the leading order approximation for the auxiliary Hermitian operator function $\hat{F}[j,p,q]$ in

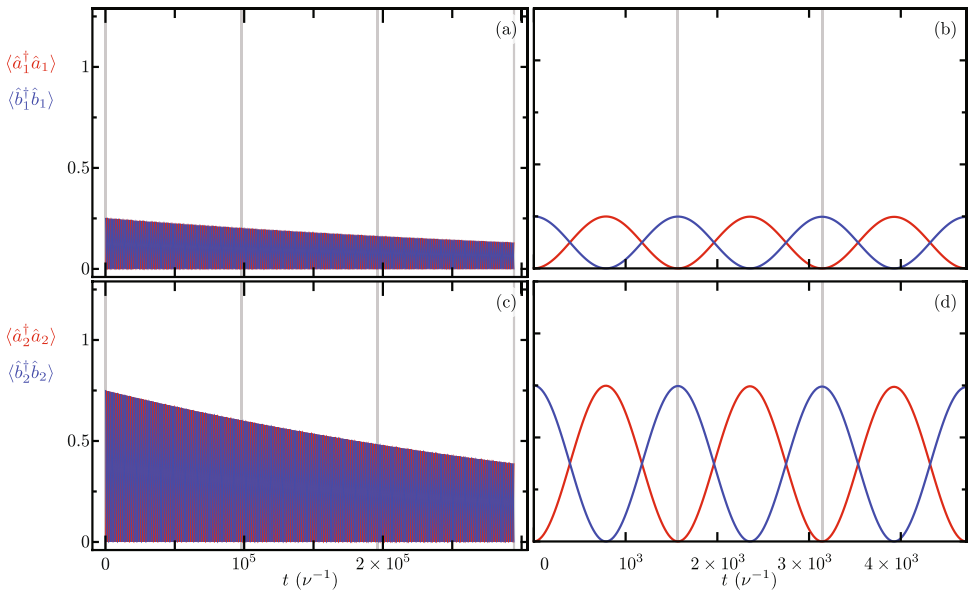

Figure 5. Time evolution of the optical, $\langle \hat{a}_j^\dagger \hat{a}_j \rangle$, and mechanical, $\langle \hat{b}_j^\dagger \hat{b}_j \rangle$, modes excitation number at each nanobeam, (**a**,**b**) $j = 1$ and (**b**,**c**) $j = 2$, for (**a**) and (**c**) long, and (**b**) and (**d**) short evolution times. The initial state is $|\psi(0)\rangle = |0,0\rangle_{\text{opt}}\left[\cos\left(\frac{\pi}{3}\right)|1,0\rangle_{\text{opt}} + \sin\left(\frac{\pi}{3}\right)|0,1\rangle_{\text{mec}}\right]$. The exchange period between (**a**) and (**c**) optomechanical modes in both nanobeams and (**b**) and (**d**) optomechanical modes in each nanobeam is indicated by vertical gray lines.

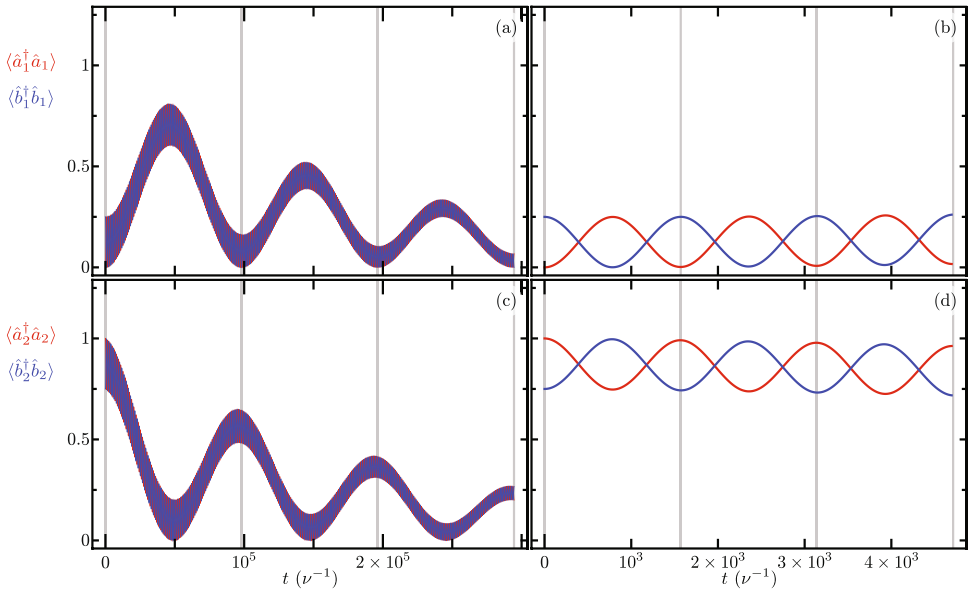

Figure 6. Same as Fig. 5 with initial state $|\psi(0)\rangle = |0,1\rangle_{\rm opt}\left[\cos\left(\frac{\pi}{3}\right)|1,0\rangle_{\rm opt} + \sin\left(\frac{\pi}{3}\right)|0,1\rangle_{\rm mec}\right]$.

Eq. (9). As in the previous section, the numerical effect of frame changes on the mean value of excitation numbers is negligible. For short, Fig. 5a and c (Fig. 6a and c), and long, Fig. 5b and d (Fig. 6b and d), evolution times with an initial state with no excitation in the optical modes, $|\psi(0)\rangle = |0,0\rangle_{\rm opt}\left[\cos\left(\frac{\pi}{3}\right)|1,0\rangle_{\rm opt} + \sin\left(\frac{\pi}{3}\right)|0,1\rangle_{\rm mec}\right]$ $\left(|\psi(0)\rangle = |0,1\rangle_{\rm opt}\left[\cos\left(\frac{\pi}{3}\right)|1,0\rangle_{\rm opt} + \sin\left(\frac{\pi}{3}\right)|0,1\rangle_{\rm mec}\right]\right)$. Figure 5b and d (Fig. 6b and d) show the predicted excitation exchange between the optical and mechanical modes in each nanobeam with frequency exchange temporal period,

$$\tau_{{\rm om},j} = 2\pi\left\{\frac{\Omega_j}{2}\left(-\frac{g_j}{\nu_j}\right)e^{-\frac{1}{2}\left(\frac{g_j}{\nu_j}\right)^2}\,{}_1{\rm F}_1\left[-\langle\hat{b}_j^\dagger\hat{b}_j\rangle;\,2;\,\left(\frac{g_j}{\nu_j}\right)^2\right]\right\}^{-1}, \tag{17}$$

that induces the exchange of mechanical excitation with a period,

$$\tau_{\rm mec} = 2\pi\left\{\gamma\left(-\frac{g_1 g_2}{\nu_1\nu_2}\right)e^{-\frac{1}{2}\left(\frac{g_1}{\nu_1}\right)^2}e^{-\frac{1}{2}\left(\frac{g_2}{\nu_2}\right)^2}\,{}_1{\rm F}_1\left[-\langle\hat{b}_1^\dagger\hat{b}_1\rangle;\,2;\,\left(\frac{g_1}{\nu_1}\right)^2\right]{}_1{\rm F}_1\left[-\langle\hat{b}_2^\dagger\hat{b}_2\rangle;\,2;\,\left(\frac{g_2}{\nu_2}\right)^2\right]\right\}^{-1}, \tag{18}$$

that can be observed in Fig. 5a and c. (Fig. 6a and c). As the evolution time in this simulation are relatively large, it is unfeasible to perform this simulation using a Lindblad formalism. We perform this simulation using a non Hermitian Hamiltonian where the diagonal imaginary parts of the Hamiltonian model optical and mechanical loss rates. For the numerical simulations in Figs. 5 and 6 we introduce the following optomechanical parameters, $\nu_1 = \nu_2 = \nu$, $g_1/\nu = g_2/\nu = 0.0004$, $\Omega_1/\nu = \Omega_2/\nu = 10$, $\Delta_1/\nu = \Delta_2/\nu = 1$, $\gamma/\nu = 400$, $\delta/\nu = 0$, $\gamma_{{\rm o},j}/\nu = 4.48 \times 10^{-6}$ and $\gamma_{{\rm m},j}/\nu = 1.39 \times 10^{-10}$. As in the previous section, the interplay between current optomechanical parameters, such as the bare coupling rate, and the loss rates reported in such devices makes it impossible to observe this phenomenon in current experimental conditions[44–46]. To observe this phenomenon either the bare optomechanical coupling should increase or the loss rates should decrease. In this numerical simulation we chose to decrease the loss rates. We set the optical loss rates to about one order of magnitude smaller than those of the record high quality factor in optical cavities[48]. We set the mechanical loss rates to the record high quality factor for mechanical resonators[49]. The rest of the parameters in this numerical simulations are consistent with our Finite Element Model. Figure 7 displays the effective couplings corresponding to the exchange of optomechanical modes in each nanobeam, Fig. 7a, and the exchange of mechanical excitation between nanobeams, Fig. 7b. The effective optomechanical coupling is independent of the optical occupation, producing overlapped data points for the first and second nanobeams, in Fig. 7a. This is the reason why temporal periods, vertical lines, in the right columns of Figs. 5 and 6 are equal. We find good agreement between our closed-form expression and data from numerical experiments. Mechanical excitation exchange, in turn, appears for nonzero values in optical occupation numbers, such as that in Fig. 6. We find good agreement between the effective coupling from our closed-form expression and results from numerical experiments. For the analyzed experimental parameter values, the effective optically controlled mechanical coupling is smaller in value than effective optomechanical coupling in each nanobeam. The numerical simulation in Fig. 7 uses the same numerical parameters as those in Figs. 5 and 6, except that the bare optomechanical coupling is variable and the losses are neglected, their effect on the effective coupling is very small.

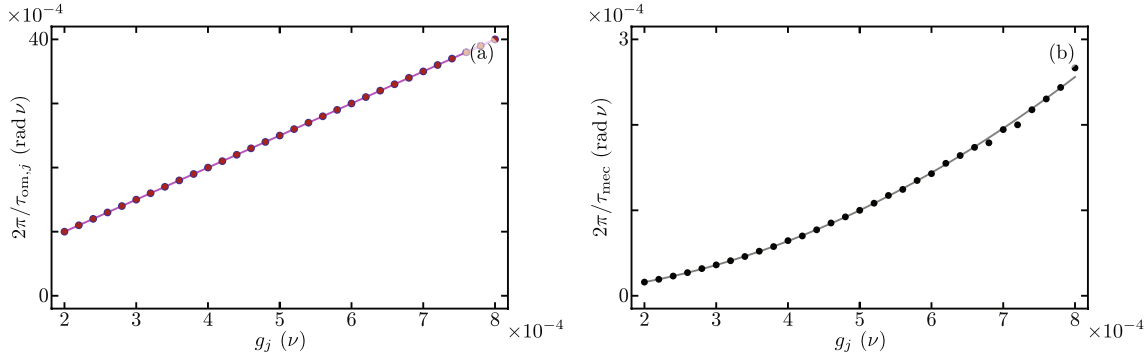

Figure 7. Effective optically controlled mechanical couplings as a function of the bare optomechanical couplings $g_j = g_1 = g_2$. (**a**) Effective optomechanical coupling in each nanobeam; the blue (red) dots are obtained from numerical experiments with a value of zero (one) in the optical occupation, and the solid curve corresponds to our closed-form expression, Eq. (17), which is independent of the optical occupation number. (**b**) Effective mechanical coupling; dots correspond to numerical experiments and the solid curve corresponds to our closed-form expression in Eq. (18).

Optically controlled mechanical two-mode squeezing

Finally, let us drive the red sideband of the optical cavities, $\Delta_j = \nu_j$, such that the optomechanical coupling terms with $q = p + 1$ satisfy the optical pumping control condition $\Delta + (p - q)\nu_j = 0$. In addition, we consider the optical cavities with a detuning equivalent to , $\delta = -\nu_1 - \nu_2$, such that the optical coupling terms with $r = s + 1$ and $u = v + 1$ satisfy the condition $\delta + (r - s)\nu_1 + (u - v)\nu_2 = 0$. Under these considerations, the effective Hamiltonian describing the system,

$$\begin{aligned}\hat{H}_{OMC} = &-\sum_j \left\{ \frac{g_j^2}{\nu_j}\left(\hat{a}_j^\dagger \hat{a}_j\right)^2 + \frac{\Omega_j}{2}\left(\hat{a}_j^\dagger F[j,2,1]\hat{b}_j + \hat{a}_j \hat{b}_j^\dagger F[j,2,1]\right)\right\} \\ &- \gamma\left\{\hat{a}_1^\dagger \hat{a}_2 \hat{b}_1^\dagger \hat{b}_2^\dagger F[1,2,1]F[2,2,1] + \hat{a}_1 \hat{a}_2^\dagger F[1,2,1]F[2,2,1]\hat{b}_2 \hat{b}_1\right\}\end{aligned} \tag{19}$$

becomes a more complex model where the first term is the standard nonlinear Kerr term, the second term is, again, linear optomechanical coupling at each nanobeam, and the third term suggest two-mode parametric coupling of the mechanical modes mediated by excitation exchange of the optical modes. Again, we used the auxiliary Hermitian operator function $\hat{F}[j,p,q]$ defined before.

Again, a first-order approximation using the coupling and pump rates ranges available for current experimental setups leads to the following effective model,

$$\hat{H}_{OMS} \approx -\sum_j \left[\frac{g_j^2}{\nu_j}\left(\hat{a}_j^\dagger \hat{a}_j\right)^2 + \Omega_{eff_j}\left(\hat{a}_j^\dagger \hat{b}_j + \hat{a}_j \hat{b}_j^\dagger\right)\right] - \Gamma_{\text{eff}}\left(\hat{a}_1^\dagger \hat{a}_2 \hat{b}_1^\dagger \hat{b}_2^\dagger + \hat{a}_1 \hat{a}_2^\dagger \hat{b}_1 \hat{b}_2\right), \tag{20}$$

where the effective linear optomechanical coupling $\Omega_{eff_j} = \Omega g_j/(2\nu_j)$ and the parametric coupling strength $\Gamma_{\text{eff}} = \gamma g_1 g_2/(\nu_1 \nu_2)$ are equal to those defined before and follow an identical hierarchy that yields the approximate effective Hamiltonian,

$$\hat{H}_{OMS} \approx -\sum_j \Omega_{eff_j}\left(\hat{a}_j^\dagger \hat{b}_j + \hat{a}_j \hat{b}_j^\dagger\right) - \Gamma_{\text{eff}}\left(\hat{a}_1^\dagger \hat{a}_2 \hat{b}_1^\dagger \hat{b}_2^\dagger + \hat{a}_1 \hat{a}_2^\dagger \hat{b}_1 \hat{b}_2\right), \tag{21}$$

whose dynamics are that of two linearly coupled optomechanical systems with an extra term that associates the exchange of optical excitation with two-mode mechanical squeezing.

Figure 8 shows the Schrödinger time evolution with a non Hermitian Hamiltonian under the effective Hamiltonian in Eq. (19) and with the leading order approximation for the auxiliary Hermitian operator function $\hat{F}[j,p,q]$. These results, just like in the two previous sections display negligible differences in the mean excitation numbers due to frame changes. Figure 8a and c show short evolution times with an initial state with no excitation in the mechanical modes, $|\psi(0)\rangle = |0,0\rangle_{\text{opt}}\left[\cos\left(\frac{\pi}{3}\right)|1,0\rangle_{\text{opt}} + \sin\left(\frac{\pi}{3}\right)|0,1\rangle_{\text{mec}}\right]$ and Fig. 8b and d for an initial state with a single excitation in the mechanical modes, $|\psi(0)\rangle = |0,1\rangle_{\text{opt}}\left[\cos\left(\frac{\pi}{3}\right)|1,0\rangle_{\text{opt}} + \sin\left(\frac{\pi}{3}\right)|0,1\rangle_{\text{mec}}\right]$, All figures show the predicted excitation exchange between optical and mechanical modes in each nanobeam with temporal period given by Eq. (17). The period related to two-mode squeezing occurs at long evolution times, which makes it unsuitable for Lindblad simulation due to the increase in excitation number provided by the two-mode squeezing. Instead we perform evolution with a non Hermitian Hamiltonian with non zero imaginary parts in the diagonal to model optical and mechanical loss rates. For the numerical simulations in Figs. 8 and 9 we introduce the following optomechanical parameters, $\nu_1 = \nu_2 = \nu$, $g_1/\nu = g_2/\nu = 0.0004$, $\Omega_1/\nu = \Omega_2/\nu = 10^{-5}$, $\Delta_1/\nu = \Delta_2/\nu = 1$, $\gamma/\nu = 400$, $\delta/\nu = -2$, $\gamma_{o,j}/\nu = 4.48 \times 10^{-6}$ and $\gamma_{m,j}/\nu = 1.39 \times 10^{-10}$. Given the interplay

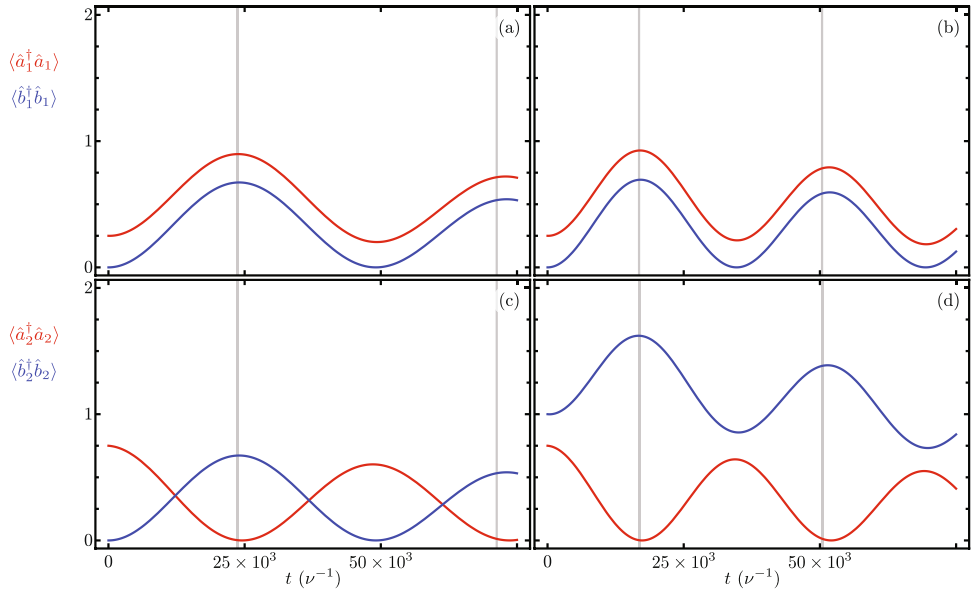

Figure 8. Time evolution of optical, $\langle \hat{a}_j^\dagger \hat{a}_j \rangle$, and mechanical, $\langle \hat{b}_j^\dagger \hat{b}_j \rangle$, modes excitation number in each nanobeam, (**a**,**b**) $j = 1$ and (**c**,**d**) $j = 2$, for initial states (**a**) and (**c**) $|\psi(0)\rangle = \left[\cos(\frac{\pi}{3})|1,0\rangle_{\text{opt}} + \sin\left(\frac{\pi}{3}\right)|0,1\rangle_{\text{opt}}\right]|0,0\rangle_{\text{mec}}$ and (**b**) and (**d**) $|\psi(0)\rangle = \left[\cos\left(\frac{\pi}{3}\right)|1,0\rangle_{\text{opt}} + \sin\left(\frac{\pi}{3}\right)|0,1\rangle_{\text{opt}}\right]|0,1\rangle_{\text{mec}}$ for short evolution times. The exchange period between optomechanical modes in each nanobeam is indicated by vertical gray lines.

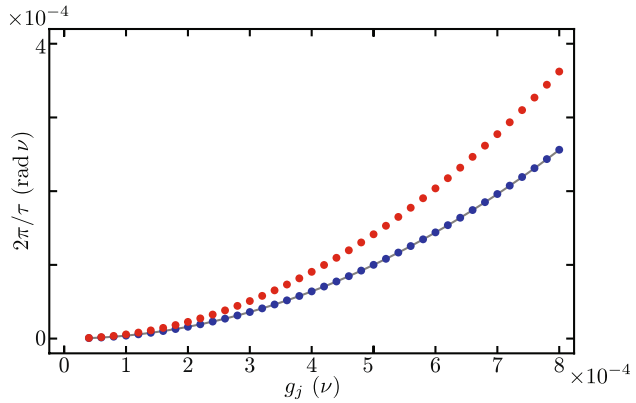

Figure 9. Parametric coupling strength Γ_{eff} for optically controlled mechanical two-mode squeezing as a function of the bare optomechanical coupling $g_j = g_1 = g_2$; blue (red) dots correspond to results from numerical experiments with a mechanical occupation value of zero (one), and the solid curve corresponds to our closed-form expression.

of current optomechanical parameters to observe the optically controlled mechanical two-mode squeezing either the bare optomechanical coupling needs to increase or the loss rates need to decrease. Like in the previous section, we decrease the optical and mechanical loss rates to the same values as before and leave the rest of the parameters in this numerical simulations consistent with our Finite Element Model. Figure 9 displays the parametric coupling strength Γ_{eff} in the optically controlled mechanical two-mode squeezing as a function of the bare optomechanical coupling $g_j = g_1 = g_2$. This coupling describes the exchange of optical and mechanical modes in each nanobeam and it also depends on the mechanical occupation numbers. We find good agreement with results from numerical experiments with a mechanical occupation value of zero and our closed-form expression. The numerical simulation in Fig. 9 uses the same numerical parameters as those in Fig. 8 except that the bare optomechanical coupling is variable and the losses are neglected, their effect on the effective coupling is very small.

Conclusion

We proposed a Hamiltonian model composed of two mechanical vibrational modes and two optical modes. The vibrational modes are mechanically isolated and coupled to their corresponding optical mode under standard optomechanical interaction. We allow for independent external driving and evanescent coupling of the optical modes. We built a finite element model of the classical problem to recover the ranges of values for variables of

interest; that is, mechanical and optical resonant frequencies for the isolated elements, their optical coupled modes, and the naked coupling strength corresponding to different configurations and separations.

We showed that our model allows the coupling of the isolated mechanical modes mediated by the optical fields. The difference between resonant frequencies of the optical modes, which may be hard to control in experimental setups, and between them and the external optical driving field frequencies control the type of mechanical interaction produced. Thanks to the ranges of parameter values, we are able to approximate the models into linear models for a small number of excitation in the system that, for example, induces an optical beam splitter where the mechanical state dresses the optical coupling, a mechanical bidirectional coupler or a two-mode squeezer where the optical state of the system controls the interaction coupling strength.

Data availability

The datasets used or analysed during the current study are available from the corresponding author on reasonable request.

Received: 2 June 2023; Accepted: 25 December 2023
Published online: 10 January 2024

References

1. Dorsel, A., McCullen, J. D., Meystre, P., Vignes, E. & Walther, H. Optical bistability and mirror confinement induced by radiation pressure. *Phys. Rev. Lett.* **51**, 155 (1983).
2. Aldana, S., Bruder, C. & Nunnenkamp, A. Equivalence between an optomechanical system and a Kerr medium. *Phys. Rev. A* **88**, 043826 (2013).
3. Cuthbertson, B. D., Tobar, M. E., Ivanov, E. N. & Blair, D. G. Parametric back-action effects in a high-Q cryogenic sapphire transducer. *Rev. Sci. Instrum.* **67**, 2435 (1996).
4. Aspelmeyer, M., Kippenberg, T. J. & Marquardt, F. Cavity optomechanics. *Rev. Mod. Phys.* **86**, 1391 (2014).
5. Mancini, S., Vitali, D. & Tombesi, P. Optomechanical cooling of a macroscopic oscillator by homodyne feedback. *Phys. Rev. Lett.* **80**, 688 (1998).
6. Marquardt, F., Chen, J. P., Clerk, A. A. & Girvin, S. M. Quantum theory of cavity-assisted sideband cooling of mechanical motion. *Phys. Rev. Lett.* **99**, 093902 (2007).
7. Marquardt, F., Clerk, A. A. & Girvin, S. M. Quantum theory of optomechanical cooling. *J. Mod. Optic.* **55**, 3329 (2008).
8. Yong-Chun, L., Yu-Wen, H., Wei, W. C. & Yun-Feng, X. Review of cavity optomechanical cooling. *Chin. Phys. B* **22**, 114213 (2013).
9. Huang, J. *et al.* Multimode optomechanical cooling via general dark-mode control. *Phys. Rev. A* **106**, 013526 (2022).
10. Weis, S. *et al.* Optomechanically induced transparency. *Science* **330**, 1520 (2010).
11. Karuza, M. *et al.* Optomechanically induced transparency in a membrane-in-the-middle setup at room temperature. *Phys. Rev. A* **88**, 013804 (2013).
12. Seok, H., Buchmann, L. F., Singh, S. & Meystre, P. Optically mediated nonlinear quantum optomechanics. *Phys. Rev. A* **86**, 063829 (2012).
13. Shkarin, A. B. *et al.* Optically mediated hybridization between two mechanical modes. *Phys. Rev. Lett.* **112**, 013602 (2014).
14. Weaver, M. J. *et al.* Coherent optomechanical state transfer between disparate mechanical resonators. *Nat. Commun.* **8**, 824 (2017).
15. Jing, H. *et al.* $\mathcal{PT}$-symmetric phonon laser. *Phys. Rev. Lett.* **113**, 053604 (2014).
16. Chen, Z. *et al.* Parity-dependent unidirectional and chiral photon transfer in reversed-dissipation cavity optomechanics. *Fundamental Res.* **3**, 21 (2023).
17. Jiang, C., Liu, Y.-L. & Sillanpää, M. A. Energy-level attraction and heating-resistant cooling of mechanical resonators with exceptional points. *Phys. Rev. A* **104**, 013502 (2021).
18. Frank, I. W., Deotare, P. B., McCutcheon, M. W. & Loncar, M. Programmable photonic crystal nanobeam cavities. *Opt. Express* **18**, 8705 (2010).
19. Qiao, Q., Xia, J., Lee, C. & Zhou, G. Applications of photonic crystal nanobeam cavities for sensing. *Micromachines* **9**, 541 (2018).
20. Zhou, J. *et al.* Refractive index sensing utilizing parallel tapered nano-slotted photonic crystal nano-beam cavities. *J. Opt. Soc. Am. B* **31**, 1746 (2014).
21. Yang, D.-Q. *et al.* Photonic crystal nanobeam cavities for nanoscale optical sensing: A review. *Micromachines* **11**, 72 (2020).
22. Pietikainen, I., Cernotik, O., Puri, S. & Filip, R. Controlled beam splitter gate transparent to dominant ancilla errors. *Quantum Sci. Technol.* **7**, 035025 (2022).
23. Gu, W. J., Yi, Z., Sun, L. H. & Yan, Y. Generation of mechanical squeezing and entanglement via mechanical modulations. *Opt. Express* **26**, 30773 (2018).
24. Li, B.-B., Ou, L., Lei, Y. & Liu, Y.-C. Cavity optomechanical sensing. *Nanophotonics* **10**, 2799 (2021).
25. Guha, B., Wu, M., Dong Song, J., Balram, K. C. & Srinivasan, K. Piezo-optomechanical actuation of nanobeam resonators for microwave-to-optical transduction. In *2021 Conference on Lasers and Electro-Optics (CLEO)*, 1 (2021).
26. Balram, K. C. & Srinivasan, K. Piezoelectric optomechanical approaches for efficient quantum microwave-to-optical signal transduction: The need for co-design. *Adv. Quantum Technol.* **5**, 2100095 (2022).
27. Braginsky, V. B. & Manukin, A. B. Ponderomotive effects of electromagnetic radiation. *Sov. Phys. J. Exp. Theor. Phys.* **25**, 653 (1967).
28. Braginsky, V. B., Manukin, A. B. & Tikhonov, M. Y. Investigation of dissipative ponderomotive effects of electromagnetic radiation. *Sov. Phys. J. Exp. Theor. Phys.* **31**, 829 (1970).
29. Xu, X.-W., Liu, Y. X., Sun, C.-P. & Li, Y. Mechanical $\mathcal{PT}$ symmetry in coupled optomechanical systems. *Phys. Rev. A* **92**, 013852 (2015).
30. Qiu, L., Shomroni, I., Seidler, P. & Kippenberg, T. J. Laser cooling of a nanomechanical oscillator to its zero-point energy. *Phys. Rev. Lett.* **124**, 173601 (2020).
31. Xue, F., Liu, Y. X., Sun, C. P. & Nori, F. Two-mode squeezed states and entangled states of two mechanical resonators. *Phys. Rev. B* **76**, 064305 (2007).
32. Tan, H., Li, G. & Meystre, P. Dissipation-driven two mode mechanical squeezing states in optomechanical systems. *Phys. Rev. A* **87**, 033829 (2013).
33. Woolley, M. J. & Clerk, A. A. Two-mode squeezing states in cavity optomechanics via engineering of a single reservoir. *Phys. Rev. A* **89**, 063805 (2014).
34. Pontin, A. *et al.* Dynamical two-mode squeezing of thermal fluctuations in a cavity optomechanical system. *Phys. Rev. Lett.* **116**, 103601 (2016).
35. Mahbood, I., Okamoto, H., Onomitsu, K. & Yamaguchi, H. Two-mode thermal-noise squeezing in an electromechanical resonator. *Phys. Rev. Lett* **113**, 167203 (2014).

36. Patil, Y. S., Chakram, S., Chang, L. & Vengalattore, M. Thermomechanical two-mode squeezing in an ultrahigh-Q membrane resonator. *Phys. Rev. Lett.* **115**, 017202 (2015).
37. Shakeri, S., Mahmoudi, Z., Zandi, M. H. & Bahrampour, A. R. Two mode mechanical non-Gaussian squeezed number state in a two-membrane optomechanical system. *Opt. Commun.* **370**, 55 (2016).
38. Martini, F. D. & Sciarrino, F. Review on non-linear parametric processes in quantum information. *Prog. Quant. Electron.* **29**, 165 (2005).
39. Piergentili, P. *et al.* Two-membrane cavity optomechanics: Non-linear dynamics. *New J. Phys.* **23**, 1367 (2021).
40. Stannigel, K., Rabl, P., Sørensen, A. S., Zoller, P. & Lukin, M. D. Optomechanical transducers for long-distance quantum communication. *Phys. Rev. Lett.* **105**, 220501 (2010).
41. Stannigel, K., Rabl, P., Sørensen, A. S., Lukin, M. D. & Zoller, P. Optomechanical transducers for quantum-information processing. *Phys. Rev. A* **84**, 042341 (2011).
42. Cole, G. D. & Aspelmeyer, M. Mechanical memory sees the light. *Nat. Nanotechnol.* **6**, 690 (2011).
43. Fiaschi, N. *et al.* Optomechanical quantum teleportation. *Nat. Photonics* **15**, 817 (2021).
44. Eichenfield, M., Chan, J., Safavi-Naeini, A. H., Vahala, K. J. & Painter, O. Modeling dispersive coupling and losses of localized optical and mechanical modes in optomechanical crystals. *Opt. Express* **17**, 20078 (2009).
45. Chan, J. *et al.* Laser cooling of a nanomechanical oscillator into its quantum ground state. *Nature* **478**, 89 (2011).
46. Chan, J., Safavi-Naeini, A. H., Hill, J. T., Meenehan, S. & Painter, O. Optimized optomechanical crystal cavity with acoustic radiation shield. *Appl. Phys. Lett.* **101**, 081115 (2012).
47. Deotare, P. B., McCutcheon, M. W., Frank, I. W., Khan, M. & Lončar, M. Coupled photonic crystal nanobeam cavities. *Appl. Phys. Lett.* **95**, 031102 (2009).
48. Wu, L. *et al.* Greater than one billion Q factor for on-chip microresonators. *Opt. Lett.* **45**, 5129 (2020).
49. Bereyhi, M. J. *et al.* Perimeter modes of nanomechanical resonators exhibit quality factors exceeding 10^9 at room temperature. *Phys. Rev. X* **12**, 021036 (2022).

Acknowledgements

F. E. O., B. R. J.-A. and F .H .M.-V. acknowledge financial support from CONACYT. F. E. O. thanks U. N. N. for study leave support.

Author contributions

B.M.R.-L. conceived the idea. F. E. O., F .H .M.-V. and B.M.R.-L. performed the analytic calculations. B. R. J.-A. performed the numeric calculations. All authors contributed to the analysis, writing, and review of the manuscript.

Funding

This study was funded by Consejo Nacional de Ciencia y Tecnología (1503245743).

Competing interests

The authors declare no competing interests.

Additional information

Correspondence and requests for materials should be addressed to B.R.J.

Reprints and permissions information is available at www.nature.com/reprints.

Publisher's note Springer Nature remains neutral with regard to jurisdictional claims in published maps and institutional affiliations.